Hindawi
Journal of Sensors
Volume 2020, Article ID 7637050, 14 pages
https://doi.org/10.1155/2020/7637050

Research Article

Self-Excited Codirectionally Magnetically Compensated Rotating Ranging Method

Pan Wu,[1] Zhiyong Guo,[2] Peng Zhang,[1] Wei Xu,[1] Zhongxiang Liu,[1] Wenhui Chen,[3] and Minghui Wei[1]

[1]*Southwest Petroleum University, College of Mechanical and Electrical Engineering, Chengdu 610500, China*
[2]*Southern University of Science and Technology, Department of Biomedical Engineering, Shenzhen 518055, China*
[3]*China Petroleum Engineering & Construction Corp Beijing Company, Beijing 100085, China*

Correspondence should be addressed to Zhiyong Guo; zhyguo@swpu.edu.cn and Minghui Wei; wmh881988@163.com

Received 23 September 2019; Revised 13 December 2019; Accepted 26 December 2019; Published 1 March 2020

Academic Editor: Paolo Bruschi

During the Steam-Assisted Gravity Drainage (SAGD) technology-based dual horizontal well drilling process, it is necessary to accurately monitor the well spacing in real time to ensure safe and parallel drilling. In this paper, a self-excited codirectionally magnetically compensated rotating ranging method and device is proposed. In the numerical calculation and simulation, both parallel and nonparallel drilling models are established. Based on the models and the magnetic dipole theory, the relation between the magnetization field and the well spacing is analyzed. Furthermore, the one-to-one correspondence between the peak-to-peak value of the magnetization field and the well spacing is revealed. Well spacing is then determined according to the measured peak-to-peak value. To achieve better results, the influence of magnetic source (the magnetic moment) and casing characteristics (magnetic susceptibility, dynamic magnetization length) on measured peak-to-peak value is analyzed. Finally, field tests are carried out, and the feasibility and effectiveness of the theory and device are proved. This study provides innovation for a new approach of magnetic guidance while drilling and has a great significance in the development, testing, and calibration of well-ranging instruments.

1. Introduction

More than 50% of global oil reserves exist in the form of heavy oil or oil sands [1]. Due to the high viscosity, the heavy oil in the oil layer is usually featured with high flow resistance and sometimes even not able to flow. Consequently, it becomes inefficient or even impossible to exploit these oil reserves using conventional oil and gas exploiting approaches [2, 3]. The safe and efficient exploiting of such unconventional oil and gas resources is of considerable significance to the national economic development. Since proposed by Butler and Stephens [4], the first time in the successful recovery of asphalt using the Steam-Assisted Gravity Drainage (SAGD) technology [4, 5], SAGD has been spread across Canada, Venezuela, and other areas with a large number of commercial applications [6, 7], which brought about considerable economic benefits. Compared with conventional exploiting methods, SAGD increased exploiting efficiency by more than 50% [8]. After that, Vapour Extraction (VAPEX) technology [5, 9, 10], solvent-assisted steam gravity drainage (Expanding-Solvent SAGD, ES-SAGD) [5–11], and other improved technologies based on SAGD further improved the exploiting efficiency of such unconventional oil and gas resources. All the exploiting techniques above are applied in the dual horizontal well model of the SAGD process: the steam injection well located above with the parallel production well located below. The well spacing is generally in the range of 4-10 m. One of the key technical points of this drilling technique is to accurately measure the well spacing in real time [12], so as to control the drilling direction and ensure the parallel drilling. If the drilling trajectory is not so well controlled, the spacing between the steam injection well and production well will vary greatly, which easily causes flashing [13].

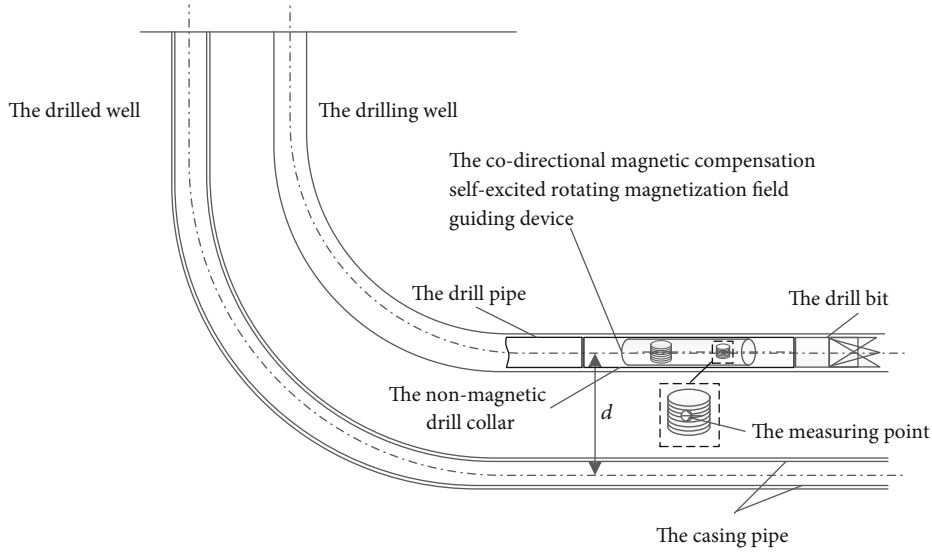

Figure 1: Dual horizontal well drilling guidance model. The upper part is the drilling well, and the lower part is the drilled well, and the codirectional magnetic compensation self-excited rotating magnetization field guiding device is located in the drilling well.

In this regard, foreign companies have developed a series of well spacing measurements and drilling guidance tools aimed at SAGD applications. Major products are Magnetic Guidance Tool (MGT) [14] and Rotating Magnet Ranging Service (RMRS) [14, 15], both of which have successfully assisted the completion of multiple SAGD dual horizontal wells in Liaohe Oilfield and Xinjiang Fengcheng Oilfield [16, 17] and exhibit good performance in drilling guidance. However, the MGT requires an electric cable to be laid in the drilled well to generate the electromagnetic field, which consequently affects the production of the drilled well, adds to the construction complexity, and increases the total cost [17]. With regard to the RMRS tool, the measuring probe must be placed downhole manually using the logging winch, and it is also required to be located right under the magnetic sub. Due to the complicated operation and the difficulty in controlling the position of the probe tube, the measurement accuracy is therefore compromised and greatly affected.

In addition to the above, Wu et al. (2014) proposed the use of a rotating magnetization field to prevent collisions during vertical well drilling and designed a magnetic compensated structure with opposite magnetic moments. Since the magnetic fields of the two magnetic sources are the same in magnitude and opposite in direction, the magnetic sensor at the midpoint of the two sources will receive zero magnetic fields in total (under the stable state of the geomagnetic field). Due to the opposite magnetic moments, the two magnetic sources induce opposite magnetization fields of the casing which cancel each other out, the overall induced magnetization field of the casing is relatively weak. The detecting and anticollision performance of this approach are therefore compromised to a certain extent. Against this, a magnetic ranging device with codirectional magnetic sources is proposed in this paper. Compared with other technologies in the drilling guidance of SAGD, the device proposed in this paper is characterized by the two codirectional magnetic sources which induce magnetization fields of the casing with the same direction; thus, a superposed magnetization field which is stronger and more easily detected by the magnetic sensor is obtained. In this way, the measurement accuracy is improved. Moreover, this method determines well spacing only based on the peak-to-peak value of the magnetization field of the casing. No auxiliary measuring equipment needs to be placed in the drilled well; therefore, no more complicated operations or procedures need to be followed. By establishing the one-to-one correspondence between the peak-to-peak value and the well spacing, the spacing can be directly found through a table or database lookup.

2. Modeling and Theoretical Derivation

2.1. Magnetic Ranging Guiding Principle. As shown in Figure 1, in the SAGD dual horizontal well drilling process, the drilling well is located above the drilled well with a well spacing of d. The self-excited codirectionally magnetically compensated rotating ranging device is installed in the nonmagnetic drill collar behind the drill bit and rotates with the bit at a low speed of 1-5 Hz [18]. A periodically varying magnetic field is generated and serves as the excitation source to magnetize the well casing. A rotating magnetization field of the casing is consequently induced. During the drilling, if the well spacing d is constant, the rotating magnetization field detected at the measuring point (at the center of the compensation electromagnet coil) is stable, and the amplitude is constant [19]. With the increase or decrease of well spacing d, the rotating magnetization field becomes unstable and varies in a negative correlation, i.e., the amplitude decreases or increases accordingly [19]. Therefore, by observing the variation of the rotating magnetization field, the trend of the well spacing can be told. Furthermore, the spacing d and the amplitude of the rotating magnetization field are in a corresponding one-to-one relation (see Case Study later for details). With a known value of the amplitude of the rotating magnetization field, the spacing can be easily found out, and the drilling direction can be subsequently decided and adjusted.

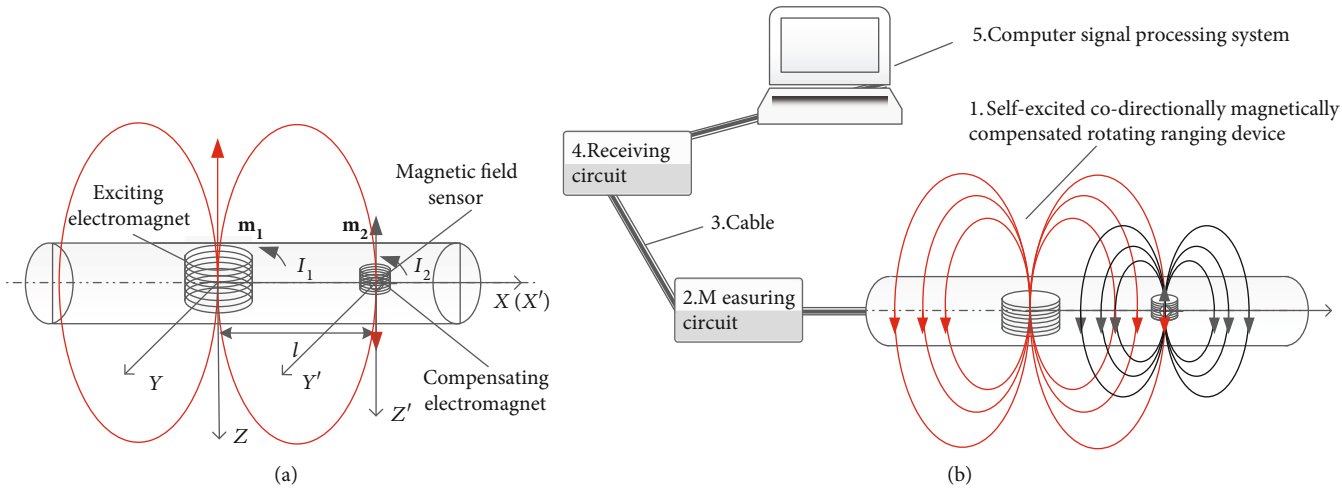

FIGURE 2: Magnetization field ranging device and data transmission processing system. (a) The structure of the codirectional magnetic compensation self-excited rotating magnetization field guiding device. It is mainly composed of an excitation electromagnet, a compensation electromagnet, and a magnetic field sensor, in which two electromagnets are placed in the same direction and the magnetic field sensor is located at the center of the compensation electromagnet coil. (b) Self-excited codirectionally magnetically compensated rotating ranging system. The ranging system is mainly composed of self-excited codirectionally magnetically compensated rotating ranging devices, measuring circuits, cables, receiving circuits, and computer signal processing systems.

2.2. Magnetic Ranging Device. As shown in Figure 2(a), the self-excited codirectionally magnetically compensated rotating ranging device is mainly composed of an exciting magnetic source of electromagnet, a codirectional compensation electromagnet, and a three-axis magnetic field sensor. The exciting magnetic source is composed of coils and an iron core, the radius of the coil is R_1, the number of turns is n_1, the current is I_1, and the amplification gain of the iron core is k. Therefore, the electromagnetic moment of the exciting magnetic source, $\mathbf{m}_1$, can be written as $n_1 I_1 k\pi {R_1}^2$. The codirectional compensation electromagnet consists only of coils, where the radius of coil is R_2, the number of turns is n_2, and the current is I_2; the magnetic moment, $\mathbf{m}_2$, is then written as $n_2 I_2 \pi {R_2}^2$. The directions of magnetic moments of the two electromagnets both follow the right-handed spiral criterion. The three-axis magnetic field sensor is installed at the center of the compensation electromagnet coil to detect the external magnetization field. The exciting electromagnet shares the same magnetic moment direction with the codirectional compensation electromagnet, so at the point of the magnetic field sensor, which locates at the interior of compensation electromagnet coils, the magnetic fields of the two electromagnets are opposite and cancel each other out. The exciting magnetic source of an electromagnet is supplied with a large current I_1, which generates an excitation field. The magnetic field of the excitation electromagnet and the codirectional compensation coil at the measuring point can be calculated by

$$\mathbf{B}_1 = \frac{\mu_0}{4\pi}\left[\frac{3(\mathbf{m}_1 \cdot l)l}{r^5} - \frac{\mathbf{m}_1}{r^3}\right], \tag{1}$$

$$\mathbf{B}_{2\mathrm{d}} = \frac{\mu_0 n_2 I_2 L_2}{\sqrt{({L_2}^2 + 4{R_2}^2)}}. \tag{2}$$

In equations (1) and (2),$\mu_0 = 4\pi \times 10^{-7}/(\mathrm{H} \times \mathrm{m}^{-1})$ is the vacuum permeability, $\mathbf{B}_1$ is the magnetic field at the excitation electromagnet in the center of the compensation electromagnet, $\mathbf{B}_2$d is the magnetic field of the codirectional compensation coil in its own center, and L_2 is the length of compensation coil. According to equation (1), magnetic intensity decreases in a negative cubic exponential manner with the increase of distance l. The excitation field becomes greatly reduced at the magnetic sensor point. On the other hand, the magnetic intensity of the compensation electromagnet reaches its maximum at the interior of the coil. That is to say, with only a small current I_2, the excitation field of the magnetic exciting source of electromagnet will be well compensated. Meanwhile, the codirectional compensation electromagnet has limited magnetic intensity externally, the magnetization field of the casing induced thereby is negligible. Therefore, it is approximately regarded that the field measured by the magnetic sensor is only the superposition of the geomagnetic field and the magnetization field of casing induced by the exciting electromagnet. Within a short period, the geomagnetic field can be regarded as stable in a small region [20], and it can be obtained by looking up values in the geomagnetic parameter table [21]. By subtracting the geomagnetic field from the magnetic sensor measured field, the magnetization field of casing induced by the exciting electromagnet is obtained. It is worth mentioning that the field can also be directly obtained using the relative measurement mode of a magnetic sensor.

As shown in Figure 2(b), it is the working principle diagram of the whole measurement system. Firstly, the device is connected to the measurement circuit. Then, the magnetic field signal is transmitted to the receiving circuit through the cable, where the signal is converted, denoised, etc. Finally, the digital signal is input to a computer data processing system for further processing to obtain information such as well spacing.

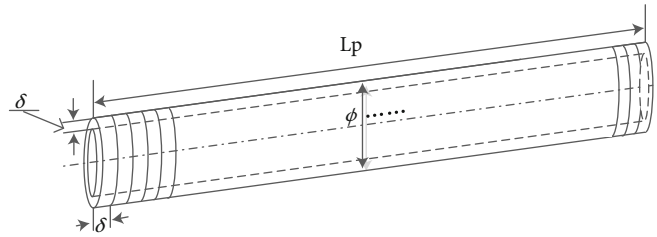

Figure 3: Unit segmentation of drilled well casing.

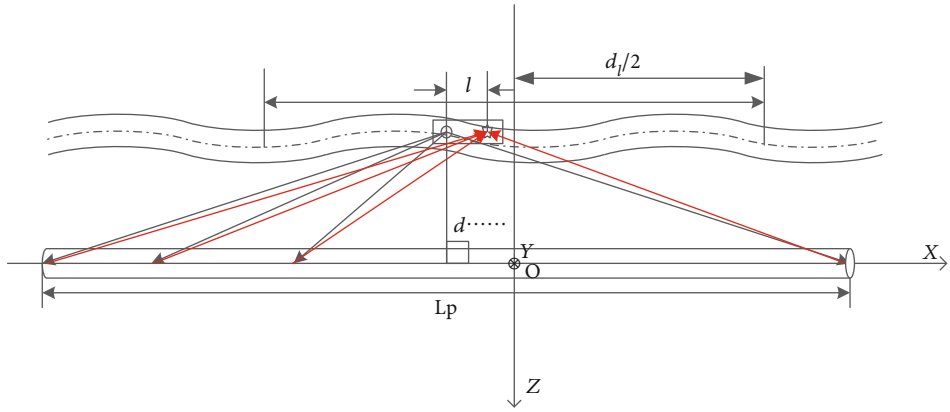

Figure 4: The coordinate system for simulation calculation.

2.3. Magnetic Ranging Theory. If the maximum geometric size of the magnetic unit is much smaller than its distance from the magnetic field measuring point, the magnetic group can be regarded as a magnetic dipole in calculation of its magnetic field. However, in the dual horizontal well model, the casing cannot be regarded as a magnetic dipole in the computation due to its nonnegligible length compared with its distance from the measuring point (4-10 m). Pignatelli et al. [22] and Guo et al. [23–25] propose that the pipeline can be segmented into small units and reconstructed thereby. The magnetic field of each segmentation unit can be calculated using the magnetic dipole method [22–24]. By performing vector superposition of the magnetic fields of all the segmentation units, the overall magnetization field of the pipeline at the measurement point can be figured out. Liu et al. [26] further propose a pipeline segmentation strategy: when the ratio of the distance from the casing to the measuring point to the casing diameter is more significant than 6.5, the pipeline can be segmented into ring-like units, and each ring will be regarded as a magnetic dipole [26]. The overall magnetic field at the measuring point will be calculated using the magnetic dipole formula. Based on the above theoretical basis, the casing is divided into units as shown in Figure 3, where the length of the casing is Lp, thickness is δ, and diameter is φ. Generally, φ is within 0.25 m. Along its axis, the casing is divided into N numbers of ring units with a step of δ, where $N = Lp/\delta$ is a ceil rounded value. The volume of each segmented unit is $V = \pi\delta^2(\varphi - \delta)/N$.

In Figure 4, a spatial rectangular coordinate system is established. In order to simulate the variation of oil well spacing d, the drilling trajectory is assumed to be sinusoidal. The drilling advances along the positive x-axis direction, the y-axis is vertically inward, and the z-axis is vertically downward. Assume that the coordinates of the measuring point are $P_j(P_{jx}, P_{jy}, P_{jz})$, $j = 1, 2, 3, \cdots$, and the coordinates of the segmentation unit are $E_i(E_{ix}, E_{iy}, E_{iz})$, $i = 1, 2, 3, \cdots, N$. The magnetic moment of exciting electromagnet $\mathbf{m}_1$ starts rotating towards the positive z-axis direction and rotates counterclockwise around the x-axis. Assume that the angle between the projection of magnetic moment in the YOZ plane and the positive z-axis direction is β, then $\mathbf{m}_1 = (0, m_1 \sin(\beta), m_1 \cos(\beta))$. The drill bit advances horizontally in a distance of d_l, and the dynamic magnetization length of the casing is m_l. When drilling reaches a certain measurement point P_j, the corresponding segmentation units are E_{1-n}. The well casing is with high magnetic susceptibility [25], and a magnetization field will be induced under the effect of the exciting electromagnet and the geomagnetic field. Since the distance from the exciting electromagnet to the drilled well casing is much larger than the maximum geometric size of the electromagnet, the exciting electromagnet can be regarded as a magnetic dipole [27]. Using the magnetic dipole formula, the magnetic field of the exciting electromagnet at the segmentation unit of casing $\mathbf{B}_{Eij}$ can be given by

$$\mathbf{B}_{Eij} = \frac{\mu_0}{4\pi}\left[\frac{3(\mathbf{m}_{1j}\cdot\mathbf{r}_{Sij})\mathbf{r}_{Sij}}{r_{Sij}^{\ 5}} - \frac{\mathbf{m}_{1j}}{r_{Sij}^{\ 3}}\right]. \tag{3}$$

In formula (3), $\mathbf{m}_{1j}$ is the magnetic moment of magnetic source at the measuring point P_j, which corresponds

to the segmentation units E_{1-i}. $\mathbf{r}_{Sij}$ is the vector from the exciting electromagnet to the segmentation unit. $r_{Sij} = \sqrt{(P_j x - E_i x)^2 + (P_j y - E_i y)^2 + (P_j y - E_i y)^2}$ is the modulus of $\mathbf{r}_{Sij}$. In consideration of the superposition of the geomagnetic field $\mathbf{B}_t$, the overall magnetic field $\mathbf{H}_{ij}$ is then given by

$$\mathbf{H}_{ij} = \frac{\mathbf{B}_{Eij} + \mathbf{B}_t}{\mu_0}, \tag{4}$$

$$\mathbf{H}_{ij} = H_{ij}x\mathbf{u} + H_{ij}y\mathbf{v} + H_{ij}z\mathbf{w}. \tag{5}$$

In equation (5), **u**, **v**, **w** are the unit vectors along the three coordinate axes of x, y, and z, respectively. The magnetic dipole is a fundamental magnetic element. The magnetic field of a ferromagnetic object can be seen as the superposition of magnetic fields of magnetic dipoles with different magnitudes [28]. The magnitude of a magnetic dipole is characterized by its magnetic moment. Under the magnetization of the external magnetic field, the nonuniform magnetic moments of the ferromagnetic unit become unified and exhibit externally in the form of the macroscopic magnetic moment [29, 30]. The ferromagnetic material of casing is magnetically isotropic, and there is no residual magnetism [6]. By assuming the magnetic susceptibility being χ_m, the magnetic moment of the ferromagnetic unit is then given by

$$\mathbf{m}_{Eij} = V \cdot \chi_m \cdot \mathbf{H}_{ij}. \tag{6}$$

By applying the magnetic dipole method, the magnetization field of the casing segmentation unit at the measuring point can be written as

$$\mathbf{B}_{ij} = \frac{\mu_0}{4\pi}\left[\frac{\mathbf{3}\left(\mathbf{m}_{Eij}\cdot\mathbf{r}_{ij}\right)\mathbf{r}_{ij}}{r_{ij}{}^5} - \frac{\mathbf{m}_{Eij}}{r_{ij}{}^3}\right]. \tag{7}$$

Equation (8) can be written as the three-component expression as follows:

$$\begin{cases} B_{ijx} = P_\kappa \cdot \left[\dfrac{\left[3H_{ijx}\left(P_{jx} - E_i x\right) + H_{ijy}\left(P_{jx} - E_{ix}\right) + H_{ijz}\left(P_{jz} - E_{iz}\right)\right]\left(P_{jx} - E_{ix}\right)}{r_{ij}{}^3} - H_{ijx}\right], \\ B_{ijy} = P_\kappa \cdot \left[\dfrac{\left[3H_{ijx}\left(P_{jx} - E_{ix}\right) + H_{ijy}\left(P_{jx} - E_{ix}\right) + H_{ijz}\left(P_{jz} - E_{iz}\right)\right]\left(P_{jy} - E_{iy}\right)}{r_{ij}{}^3} - H_{ijy}\right], \\ B_{ijz} = P_\kappa \cdot \left[\dfrac{\left[3H_{ijx}\left(P_{jx} - E_{ix}\right) + H_{ijy}\left(P_{jx} - E_{ix}\right) + H_{ijz}\left(P_{jz} - E_{iz}\right)\right]\left(P_{jz} - E_{iz}\right)}{r_{ij}{}^3} - H_{ijz}\right]. \end{cases} \tag{8}$$

In equation (8), $P_\kappa = u_0\delta^3(\varphi - \delta)\chi_m/4\mathrm{L}\mathrm{p}r_{ij}{}^2$, $r_{ij} = \sqrt{(P_{jx} - (E_{ix} - l))^2 + (P_{jy} - E_{iy})^2 + (P_{jy} - E_{iy})^2}$.

Based on vector superposition, the overall magnetization field of casing segmentation units at the measurement point $\mathbf{B}_j$ is calculated as

$$\mathbf{B}_j = \sum_{i=1}^{N} \mathbf{B}_{ij}. \tag{9}$$

Since the geomagnetic field and the fluctuation of the electromagnetic field are stable, so the signal measured by the magnetic sensor working in a relative measurement mode is only the fluctuating magnetization field induced by the electromagnetic source, namely,

$$B_m = \left|\mathbf{B}_j\right|. \tag{10}$$

3. Numerical Simulation Analysis

3.1. Model Parameter Characterization. The magnetic moment of exciting electromagnet is characterized by the coil area S, the number of turns n, the current I_1, and the magnification gain of the iron core k. In the simulation model, the coil radius R_1 is 4 cm, the number of turns n is 2000 rpm, the current I_1 is 10 A, and the magnification gain k is 500. So the magnetic moment, which is expressed as m_0, is calculated to be $5.0265 \times 10^4(\mathrm{A}\cdot\mathrm{m}^2)$. The distance from the exciting electromagnet center to the magnetic sensor l is 20 cm. The coil radius of the compensation solenoid R_2 is 3 cm, the number of turns n is 1000 rpm, the current I_1 is 6 A, and the magnification gain k is 100. The magnetic moment is then calculated to be $282.7(\mathrm{A}\cdot\mathrm{m}^2)$. The geomagnetic parameters of Daqing Oilfield are adopted in the simulation; the total geomagnetic intensity is 55972.5 nT, the geomagnetic dip is 64.285°, and the geomagnetic declination is -10.383° [31]. The casing magnetic susceptibility χ_m is 300, casing outer diameter φ is 114.3 mm, and thickness δ is 10 mm. The distance that the drill bit advances d_l is 6 m. By taking one measuring point every 0.0003 m, the total number of measuring points is 240001. The dynamic magnetization length of casing m_l is 80 m.

3.2. Case Study. When the drilling is parallel to the drilled well, the well spacing is constantly 4 m. The numerical simulation results in Figure 5(a) show that the amplitude of the magnetization field remains unchanged and the peak-to-

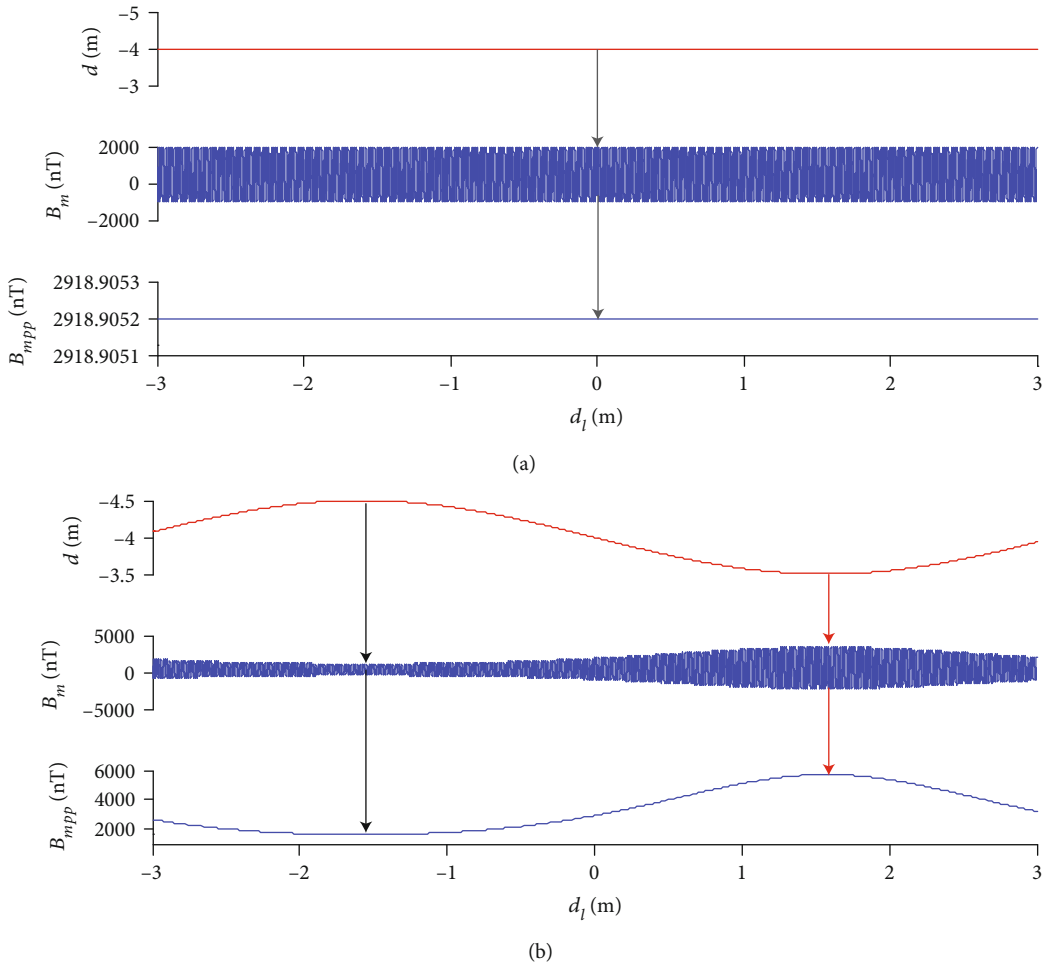

Figure 5: Magnetization field of different drilling models. (a) Magnetization field in parallel drilling. (b) Magnetization field in sinusoidal nonparallel drilling. In both two figures, the top red curve is the drilling well track, the middle graph is the fluctuation trend of the magnetization field, and the bottom blue curve is the peak-to-value of the magnetization field.

peak value (wave peak to wave valley), expressed as B_{mpp}, is constant due to the constant distance d from the measuring point to the casing axis. For simulation of nonparallel drilling, a sinusoidal drilling trajectory is adopted to simulate the possible approaching and departure of drilling well towards the drilled well. The sinusoidal trajectory reflects the variation of a drill bit in practical drilling engineering; therefore, this nonparallel drilling model established is reasonable and of practical significance. Assume that the amplitude of the sinusoidal trajectory is 0.5 m, the minimum distance to the drilled well is 3.5 m, and the maximum distance is 4.5 m. The simulation is conducted with results shown in Figure 5(b). As the figure shows, the peak-to-peak value gradually increases when well spacing decreases. When the distance is minimum ($d = 3.5$ m), the peak-to-peak value reaches its maximum (refer to the curve section between the black and red arrows). When well spacing increases, the peak-to-peak value gradually decreases. With the maximum distance ($d = 4.5$ m), the peak-to-peak reaches its minimum. The peak-to-peak value is only related to the well spacing d. Therefore, it is possible to accurately tell whether the two wells are parallel, approaching, or departing from each other according to the magnetization field waveform.

It is known from Figure 5 that there is a specific correlation between the peak-to-peak value and well spacing d. To further study the correlations, since SAGD dual horizontal well spacing is usually in the range of 4-10 m and the magnetization field strength at the measuring point is less than 1 nT when d is more than 20 m (Figure 6(b)), which is below the sensor resolution and cannot reflect the target magnetic field characteristics completely, the well spacing is assumed to be in the range of 0.5-20 m, the peak-to-peak value is analyzed when the well spacing varies with a step of 0.2 m. The results are shown in Figure 6. As can be seen from Figures 6(a) and 6(b), as the well spacing d gradually increases, the peak-to-peak value gradually decreases and exhibits a one-to-one correspondence with the well spacing d. For well spacing $0 < d < 5$ m, the peak-to-peak value sharply attenuates with the increase of distance (10^7- > 10^2 nT), which reveals that under circumstances of small well spacing, the magnetization field of casing induced by the self-excitation source is relatively strong, the peak-to-peak signal is more easily to

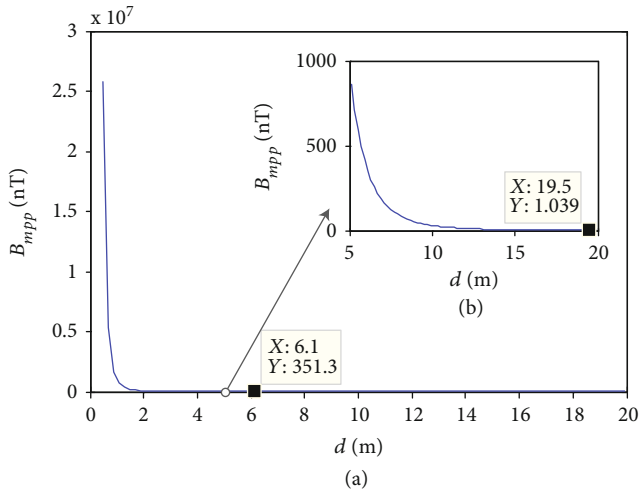

FIGURE 6: Attenuation of the peak-to-peak value in accordance with well spacing. (a) shows the attenuation process of magnetic field peak-to-peak value along with well spacing from 0.5 m to 20 m; (b) shows the magnification of magnetic field peak-to-peak value attenuation during the 5-20 m well spacing variation in (a).

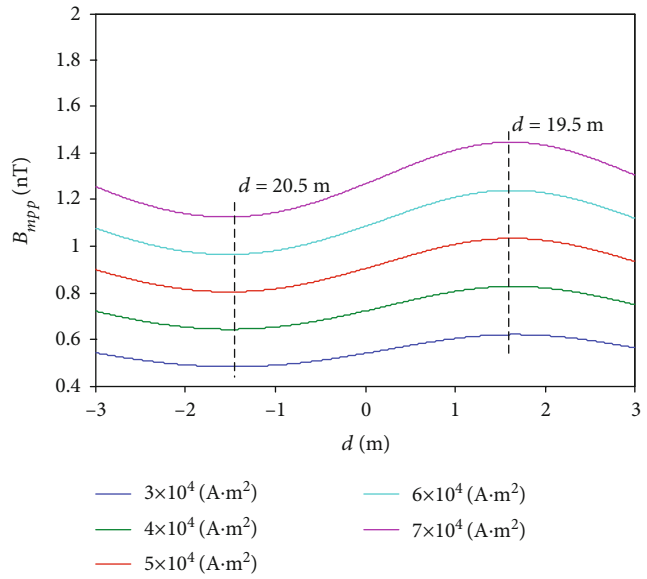

FIGURE 7: The variation trend of peak-to-peak value in accordance with magnetic moment and well spacing.

be detected, and therefore, the well distance will be calculated more accurately. For well spacing larger than 5 m, the peak-to-peak value attenuates moderately. When $d = 19.5$ m, the peak-to-peak value attenuates to 1.039 nT, which is merely strong enough to be recognized by the magnetic field sensor. Therefore, it can be judged that the theoretical effective measurement range based on the current model is about 0-19 m. By increasing the magnetic moment of the electromagnet (increasing the number of coil turns, the coil radius, the current supply, and the core magnification), the effectively recognizable range of the magnetization field will be further extended. According to the analysis above, it is clear that by placing measuring points with relatively smaller step length (for example, 0.01 m) and establishing a lookup table database defining the correlation between peak-to-peak value and well spacing d, the well spacing can be easily found out according to the measured peak-to-peak value. For example, the measured peak-to-peak value is 351.3 nT. According to the existing lookup table database, it can be found that the well spacing is about 6.1 m.

4. Influencing Factors of Magnetization Field

When calculating the magnetization field of the casing at the measuring point, many factors affect the calculation result. Major factors are the exciting electromagnet and the casing. The exciting electromagnet influences through its magnetic moment **m**. While the casing influences through parameters such as casing susceptibility χ_m, dynamic magnetization length Lp, and casing diameter φ. By assuming that the stratum is uniform and ignoring the magnetic minerals in stratum around the casing, the influence of the abovementioned factors on the magnetization field is studied.

4.1. Influences of the Exciting Electromagnet. The exciting electromagnet is the fundamental source of the peak-to-peak signal of the rotating magnetization field, which directly affects the measurement range and accuracy. The larger the magnetic moment of the electromagnet **m**, the stronger the rotating magnetization field, the more severe the magnetic fluctuation, and the easier it is to be collected by the magnetic sensor. According to the calculation formula, the magnetic moment of the electromagnet **m** is dependent on the coil radius, the number of coil turns, the magnification gain, and the current supply. Therefore, the current supply I and number of turns n should be increased as much as possible to generate a larger magnetic moment. For the simulation model established before, the magnetic moment m is calculated to be $5.0265 \times 10^4 (\mathrm{A} \cdot \mathrm{m}^2)$. On this basis, here m is assumed to be 3×10^4, 4×10^4, 5×10^4, 6×10^4, and 7×10^4 $(\mathrm{A} \cdot \mathrm{m}^2)$respectively, to conduct further simulation studies. Assume that $d_l = 6$ m, $Lp = 80$ m, the drilling follows the sinusoidal nonparallel model as shown in Figure 5(b), and the well spacing d ranges between 19.5 and 20.5 m (from the previous numerical simulation results, the maximum theoretical detection range is 19.5 m). As can be seen from Figure 7, the simulation results show that with the same drilling trajectory (the well spacing d varies consistently), the peak-to-peak values of magnetization fields induced by different magnetic moments share the same variation trend. With the same well spacing d (such as $d = 20.5$ m or $d = 19.5$ m), the peak-to-peak value increases with the increase of magnetic moment. Therefore, if condition permits, electromagnet with a more significant magnetic moment should be employed to induce stronger peak-to-peak signals and improve measurement accuracy.

4.2. Influence of Casing Characteristics

4.2.1. Magnetic Susceptibility. The casing acts as a "transfer" media of the magnetic field of exciting electromagnet. The magnetic susceptibility thereof will directly determine the

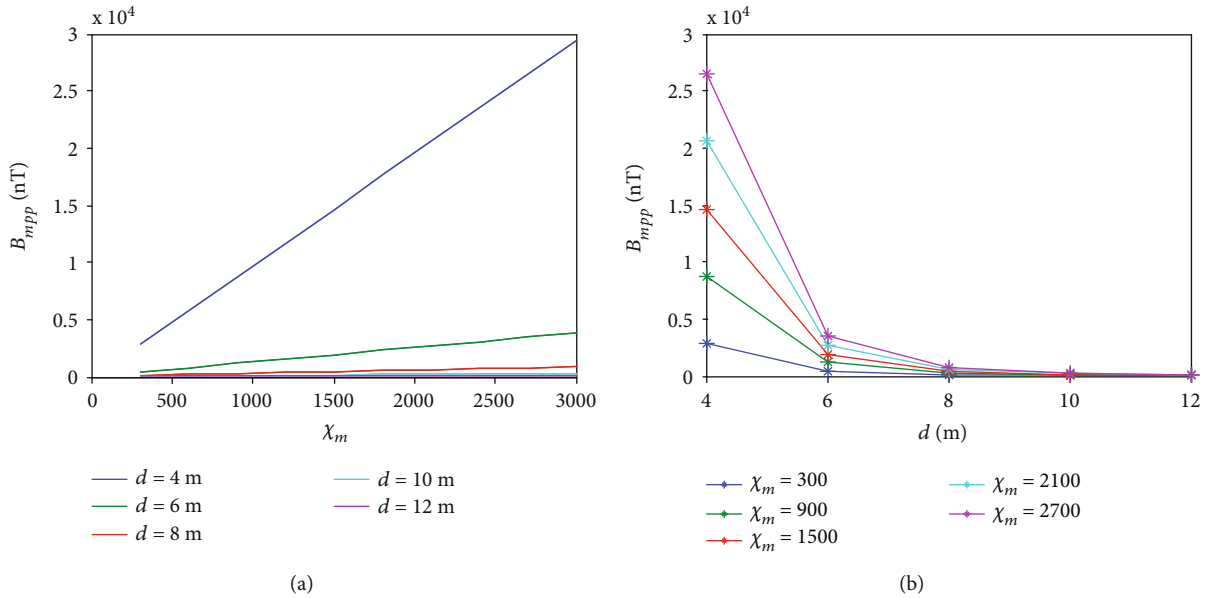

FIGURE 8: Influence of magnetic susceptibility on peak-to-peak value. (a) shows the variation rule of the peak value of the magnetization field with the magnetic susceptibility at different well spacing; (b) shows the effect of well spacing on the peak value of the magnetization field at different magnetic susceptibility.

transfer amount and efficiency. The magnetic susceptibility of ferromagnetic materials is generally with the order of 10-10^6, while that of the ferromagnetic material is generally between 10 and 10^3. In this chapter, the magnetic susceptibility χ_m is assumed as variable while parameters of the exciting electromagnet remain constant. The parallel drilling model is adopted. The value of χ_m varies between 300 and 2700 with a step of 300. On the other hand, during a drilling distance of 6 m, the well spacing is assumed to change from 4 to 12 m with a step of 2 m. Based on these assumptions, the peak-to-peak value of the magnetization field is calculated. The simulation results are shown in Figure 8. It can be seen from Figure 8(a) that when the well spacing d is constant, the peak-to-peak value increases linearly with the increase of magnetic susceptibility χ_m. While from Figure 8(b), it can be observed that under certain magnetic susceptibility χ_m and drilling distance d_l, the peak-to-peak value decreases and attenuates exponentially with the increase of well spacing d. Therefore, it can be deduced that with relatively larger magnetic susceptibility, the casing will be able to generate more severe magnetic fluctuations, which will be more easily captured by the magnetic sensor and thus contributing to a more accurate calculation of well spacing.

4.2.2. Dynamic Magnetization Length of the Casing. The dynamic magnetization length of the casing is a nonnegligible influencing factor. According to Biot-Savart's law, the magnetic intensity decreases in a negative cubic exponential manner with the increase of distance. When a certain length of casing is magnetized by the magnetic source, the magnetic sensor collects the overall magnetization field signal of the casing segment. The dynamic magnetization length of casing will directly determine how much signal will be received by the sensor and thus affecting the peak-to-peak value of the signal. With a reasonable dynamic magnetization length, measurement error and amount of computation can be effectively reduced, and the calculation speed and accuracy will be greatly improved. When $d = 4$ m, $\chi_m = 300$, and $m_1 = m_0$, measurements of magnetization field are carried out at several randomly selected measuring points, i.e., the 1000^{th}, 2000^{th}, 3000^{th}, 5000^{th}, 8000^{th}, and 15000^{th} measurement points. For each measuring point, dynamic magnetization length ranging from 0 to 300 m with a step of 1 m is adopted. As the measurement results in Figure 9 show, for dynamic magnetization length of casing out of a certain range (greater than 80 m), the geomagnetic field will become the major source of magnetization. Under such circumstances, the peak-to-peak value will remain almost unchanged even if the dynamic magnetization length of casing further expands, due to the nearly constant state of geomagnetic field. Therefore, a dynamic magnetization length of 80 m is considered to be enough and reasonable. The magnetic moment of the exciting electromagnet constantly changes its direction due to the rotation. At the 3000^{th} and 15000^{th} measuring points, the projection of magnetic moment forms an included angle of $0 - 180^\circ$ with the positive z-axis on the YOZ plane, so the induced magnetization field is also positive, and the value gradually increases to a stable value. On the other hand, at the 1000^{th}, 2000^{th}, 5000^{th}, and 8000^{th} measurement points, the projection of magnetic moment forms a $0 - (-180^\circ)$ included angle with the positive the z-axis on the YOZ plane, the magnetization field induced thereby becomes negative accordingly, and the value gradually decreases to a stable value.

5. Field Test Analysis and Discussion

5.1. Experimental Analysis. The field test was carried out in a certain area of Xindu District of Chengdu (N30°49′43.66,

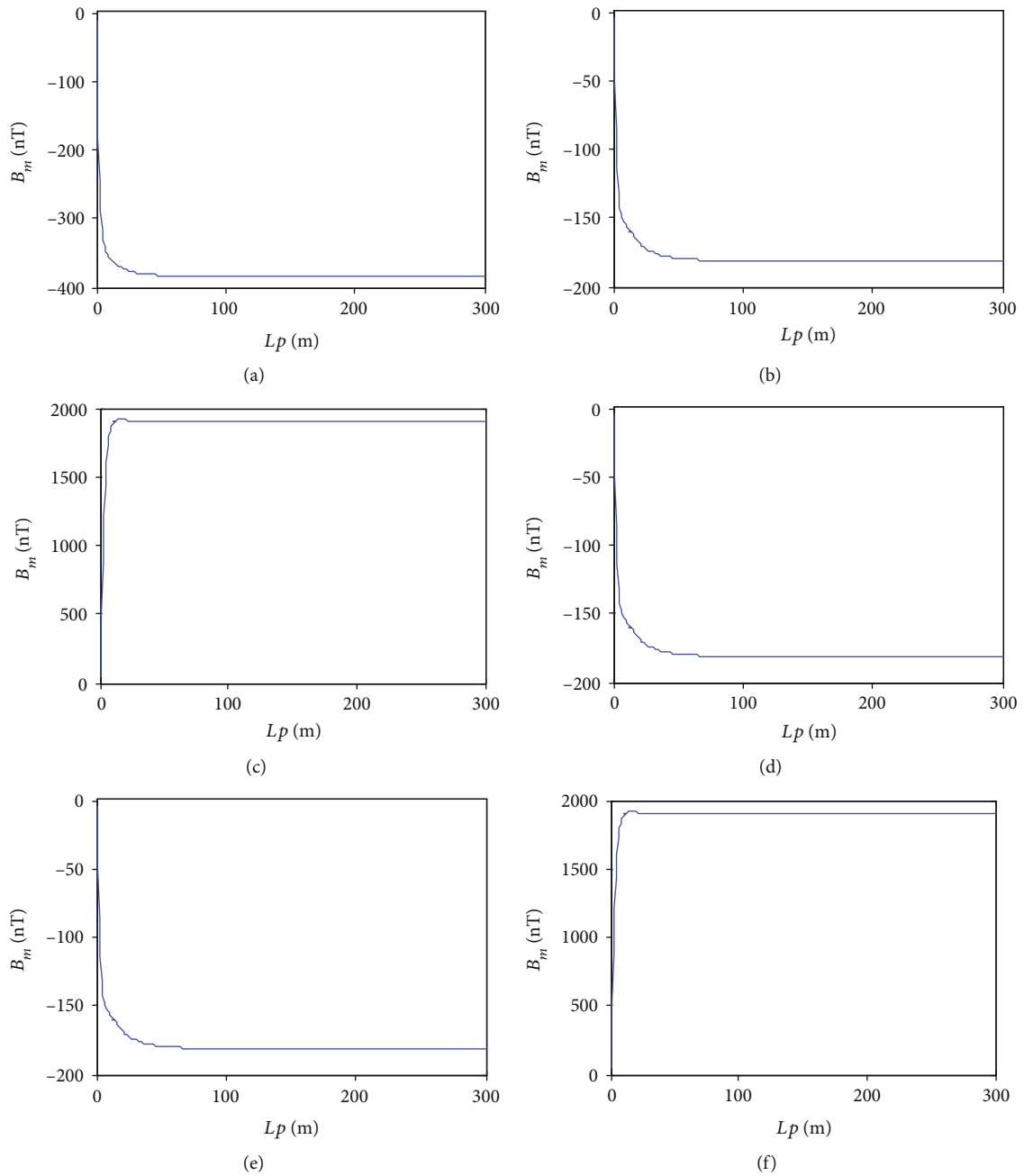

Figure 9: Influence of dynamic magnetization length of the casing on magnetization field. (a)–(f) show the variation of the magnetization field during the change of the dynamic magnetization length of the casing from 0 to 300 m at the 1000th, 2000th, 3000th, 5000th, 8000th, and 15000th measuring points, respectively.

E104°10′55.38″). The average geomagnetic intensity measured in this area is 56430 nT. Due to the limited test conditions, a cylindrical permanent magnet was used instead of the electromagnet. Compared with the electromagnet, a similar magnetization effect can be achieved using the permanent magnet. The only difference lies in the magnetic intensity (the magnetization field of the permanent magnet is smaller than that of the electromagnet). The cylindrical magnet is 60 mm high, the bottom diameter is 50 mm, and the residual magnetism is 1.2 T. The weak magnetic detection sensor employed is a CH-330 high-precision digital fluxgate meter, which is with a resolution of 1 nT and a range of ±100 μT. The adopted sensor is enough to meet all measurement requirements. In this test, parallel drilling and nonparallel drilling were studied separately. The magnetic moment of the permanent magnet is relatively small, and it attenuates and becomes even less with the increase of measuring distance. In order to achieve better measurement results, the dual well model with a well spacing of 1 m was finally configured and set up. Along the drilling distance of

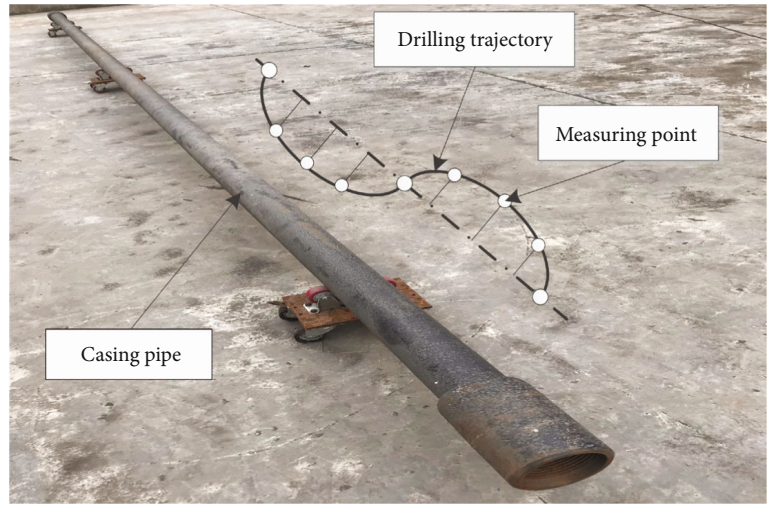

Figure 10: Experimental site in a specific area of Chengdu.

1 m, measuring points are specified every 0.05 m. As Figure 10 shows, the drill bit rotates in a round at each measuring point. By conducting the interpolation processing, the magnetization fields are obtained and shown in Figure 11. The magnetic field is shown in Figure 11(a) which is the geomagnetic field that the sensor detects when it rotates at a certain measuring point. Theoretically, within a short time, the geomagnetic field should be constant for a particular region. But due to the internal coil structure of the sensor itself, the measured geomagnetic field is periodically changing other than constant. Therefore, by simply subtracting a constant geomagnetic field value from the measured magnetization field of the sensor, a sinusoid not so completely symmetrical will be obtained. As shown in Figure 11(b), the positive half is wider than the negative half of the curve. From Figures 11(c)–11(e), it is clear that the test results are consistent with the theoretical analysis. For both parallel and nonparallel dual well models, the magnetization field undergoes the same trend as theoretically analyzed. If the well spacing remains unchanged, the amplitude of the magnetic fluctuation wave remains unchanged. The peak-to-peak value of the magnetization field is negatively correlated with the well spacing and the correlation falls into a corresponding one-to-one mode. According to the field tests, the magnetic ranging theory proposed in this paper is well proved.

5.2. Discussion and Comparison. The above experimental has verified the feasibility and effectiveness of self-excited codirectionally magnetically compensated rotating ranging method. Compared with the existing leading magnetic guiding technologies MGT and RMRS applied to SAGD dual horizontal well, it has the following four characteristics:

(1) Magnetic beacon: the magnetic beacons of the MGT and the RMRS tool are electric solenoid and the permanent magnet stub, respectively, that of the ranging device mentioned in this paper is the energized coil. The above three methods are active magnetic source beacons, in which magnetic field strength is enormous, and the value can be calculated relatively accurately, so the measurement accuracy and range are tremendous. The magnetic field strength is significant, and the size can be calculated accurately. Therefore, measuring precision and scope are bigger

(2) Accuracy: from the analysis of three ranging guidance principles, it is known that MGT and RMRS directly use the sensor to detect the magnetic source signal. During the process, the magnetic measurement will inevitably be affected by the magnetic field of ferromagnetic materials such as drill pipe and casing (and the screen pipe). Self-excited codirectionally magnetically compensated rotating ranging method uses the codirectional coil to shield the magnetic source magnetic field at the position of the sensor, so the measured data is the superimposed data of the magnetization field and the geomagnetic field, and as the geomagnetic field has a constant value, the magnetization field can be directly obtained. The other influencing factors of the process (mineral magnetic field, etc.) are small, so the measurement accuracy is higher in principle

(3) Time-consuming: when the MGT drills into a certain distance, it needs to stop drilling for single-point signal data analysis, which takes much time. At the same time, the magnetic signal detection tool is more than 10 m away from the drill bit and cannot accurately reflect the position of the drill bit relative to the drilled hole. However, our ranging method need not stop drilling, can do both real-time measurement and single-point measurement at the same time, saving drilling time

(4) Cost: MGT needs to be placed in the drilled well to generate electromagnetic signals through a cable power supply, while the RMRS tools also need to place a measuring tube in the drilled well to realize magnetic signal acquisition and communication, which undoubtedly increases the production costs

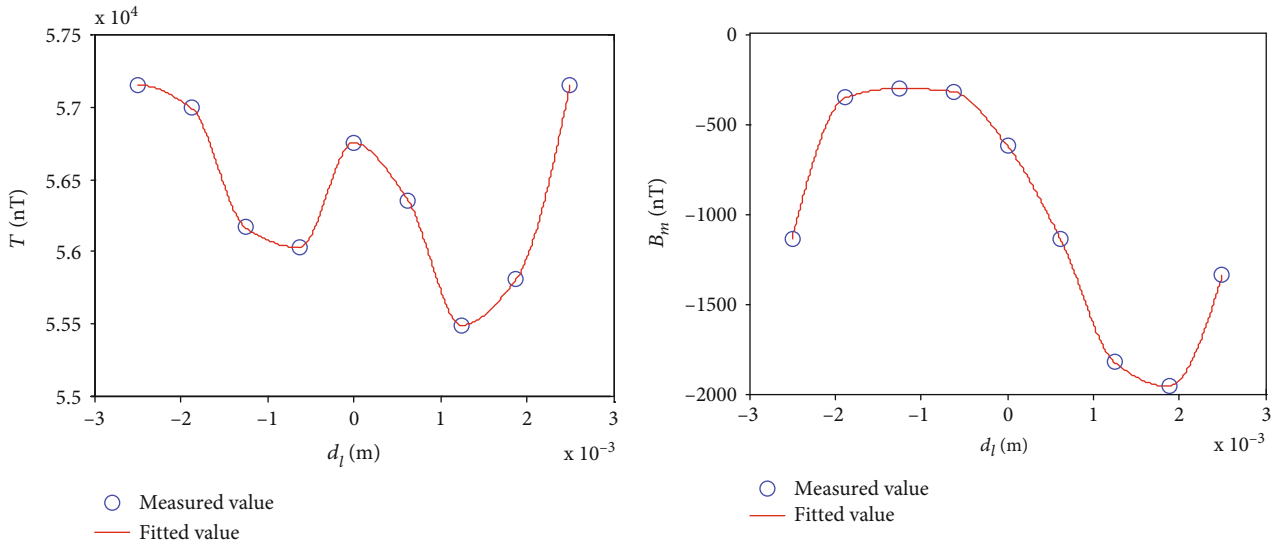

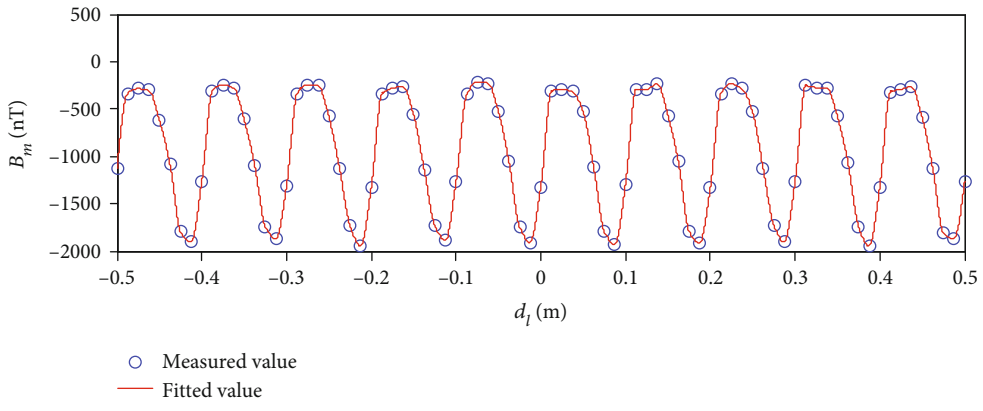

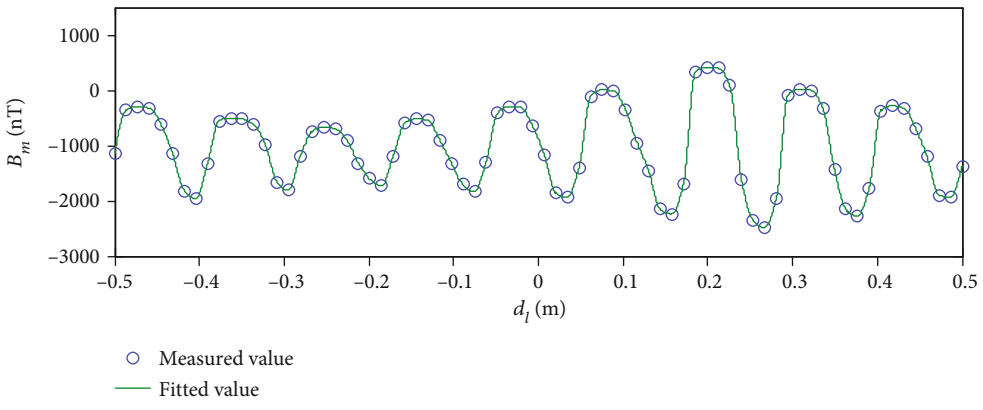

Figure 11: Continued.

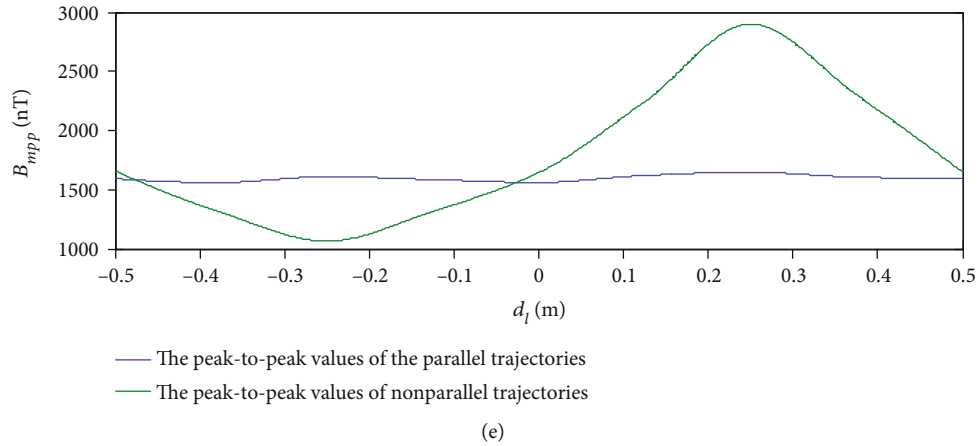

(e)

FIGURE 11: Field test data with curve fitting. (a) Rotating geomagnetic field. (b) One cycle of magnetization field curve at a certain measuring point. (c) Magnetization field curve of parallel drilling. (d) Magnetization field curve of nonparallel drilling. (e) The peak-to-peak value of parallel and nonparallel drilling trajectories.

and affects the drilling process. Instead, a self-excited codirectionally magnetically compensated rotating ranging method only needs to install the measuring equipment under the drilling well, and it is not necessary to enter other equipment in the drilled well, which can greatly improve the production efficiency

6. Conclusion

In this paper, a self-excited codirectionally magnetically compensated rotating ranging device is proposed. The casing is segmented into small groups. By applying the magnetic dipole theory to the segmented units, the overall magnetization field of the casing at a certain measurement point is calculated.

(1) According to the calculation, the relationship between the peak-to-peak value of the magnetization field and the well spacing is studied and established. Furthermore, influences of exciting electromagnet parameters and casing parameters on the peak-to-peak value are simulated

(2) It is suggested by the simulation from the peak-to-peak value. It can be effectively determined whether the two wells are approaching or departing from each other. Since the peak-to-peak value and well spacing are one-to-one corresponding, the well spacing can be directly found out according to the peak-to-peak value if a lookup table database is established

(3) If the condition permits, the accuracy and range of this ranging method can be improved by increasing the magnetic moment. According to the study, a dynamic magnetization length of a casing of 80 m will effectively reduce the measurement error and the computation load

Through the simulation and field tests, the magnetic ranging device proposed in this paper is found to be practical and reliable. Moreover, it provides a new idea for the development of LWD instruments.

Nomenclature

d: The well spacing
R_1: The coil radius of the excitation electromagnet
n_1: Number of turns of excitation electromagnet coil
I_1: Current of the excitation electromagnet coil
k: Core magnification
$\mathbf{m}_1$: The magnetic moment of the excitation electromagnet
R_2: Coil radius coaxial compensation solenoid
n_2: Number of turns of the coaxial compensating electromagnet coil
I_2: Compensating coil current of the electromagnet
$\mathbf{m}_2$: Compensating electromagnet magnetic moment
Lp: The length of casing
δ: The thickness of the casing
φ: The casing diameter
N: Number of the segmentation unit
β: The angle formed by the projection of $\mathbf{m}_1$ in plane YOZ and the positive direction of the z-axis
μ_0: Vacuum permeability
$\mathbf{m}_{2i}$: The magnetic moment of the permanent magnet magnetic source at the measuring point
$\mathbf{r}_{Sij}$: Location vector of the magnetic source to casing the segmentation unit
$\mathbf{B}_t$: Geomagnetic field
$\mathbf{H}_{ij}$: Superimposed field strength
$\mathbf{u}$,$\mathbf{v}$,$\mathbf{w}$: Unit vectors of x, y, and z axes, respectively
χ_m: Casing susceptibility
$\mathbf{B}_j$: The magnetic field at the measuring point of the segmentation unit
B_m: Magnetization field
d_l: Drilling distance
B_{mpp}: Peak-to-peak value of the magnetization field.

Data Availability

(1) The data (geometric model) used to support the findings of this study are included in the article. (2) The data (influencing factors of magnetization field) used to support

the findings of this study are included in the article. (3) The data (figures) used to support the findings of this study are included in the article.

Conflicts of Interest

The authors declare that there are no conflicts of interest regarding the publication of this paper.

Acknowledgments

This work is supported by the National Natural Science Foundation of China under Grant (No. 41374151) and the Sichuan Province Applied Basic Research Project (No. 2017JY0162).

References

[1] D. Ji, H. Zhong, M. Dong, Z. Chen, and X. Jia, "A model to estimate heat efficiency in steam-assisted gravity drainage by condensate and initial water flow in oil sands," *Industrial & Engineering Chemistry Research*, vol. 55, no. 51, pp. 13147–13156, 2016.

[2] A.-M. Al-Bahlani and T. Babadagli, "SAGD laboratory experimental and numerical simulation studies: a review of current status and future issues," *Journal of Petroleum Science and Engineering*, vol. 68, no. 3-4, pp. 135–150, 2009.

[3] B. Li, Y. Fan, Z. Sun, Z. Wang, and L. Zhu, "Effects of high-frequency pulsed electrical field and operating parameters on dehydration of SAGD produced ultra-heavy oil," *Powder Technology*, vol. 316, pp. 338–344, 2017.

[4] R. M. Butler and D. J. Stephens, "The gravity drainage of steam-heated heavy oil to parallel horizontal wells," *Journal of Canadian Petroleum Technology*, vol. 20, no. 2, p. 8, 1981.

[5] D. Voskov, R. Zaydullin, and A. Lucia, "Heavy oil recovery efficiency using SAGD, SAGD with propane co-injection and STRIP-SAGD," *Computers & Chemical Engineering*, vol. 88, pp. 115–125, 2016.

[6] V. Sanchez, Yaoguo Li, M. N. Nabighian, and D. L. Wright, "Numerical modeling of higher order magnetic moments in UXO discrimination," *IEEE Transactions on Geoscience and Remote Sensing*, vol. 46, no. 9, pp. 2568–2583, 2008.

[7] O. Mohammadzadeh, N. Rezaei, and I. Chatzis, "Pore-level investigation of heavy oil and bitumen recovery using solvent –aided steam assisted gravity drainage (SA-SAGD) process," *Energy & Fuels*, vol. 24, no. 12, pp. 6327–6345, 2010.

[8] L. Q. Yang, Y. M. Chen, H. Wang, and L. Tian, "Physical and numerical simulation of steam-assisted gravity drainage with vertical and horizontal well combination in extra heavy oil reservoir," *Journal of China University of Petroleum(Edition of Natural Science)*, no. 4, pp. 64–69, 2007.

[9] M. Butler Roger and I. J. Mokrys, "Recovery of heavy oils using vapourized hydrocarbon solvents: further development of the Vapex process," *Journal of Canadian Petroleum Technology*, vol. 32, no. 6, p. 8, 1993.

[10] L. A. James, N. Rezaei, and I. Chatzis, "VAPEX, warm VAPEX, and hybrid VAPEX-the state of enhanced oil recovery for in situ heavy oils in Canada," in *Canadian International Petroleum Conference*, p. 9, Calgary, Alberta, 2007.

[11] T. N. Nasr and E. E. Isaacs, "Process for enhancing hydrocarbon mobility using a steam additive," 2001, U.S. Patent No. 6,230,814.

[12] B. B. Diao, D. L. Gao, and Z. Y. Wu, "Magnet ranging calculation method of twin parallel horizontal wells steerable drilling," *Journal of China University of Petroleum(Edition of Natural Science)*, vol. 35, no. 6, pp. 71–75, 2011.

[13] S. K. Das, "Well bore hydraulics in a SAGD well pair," in *SPE International Thermal Operations and Heavy Oil Symposium*, p. 6, Calgary, Alberta, Canada, 2005.

[14] T. L. Grills, "Magnetic ranging technologies for drilling steam assisted gravity drainage well pairs and unique well geometries - a comparison of technologies," in *SPE International Thermal Operations and Heavy Oil Symposium and International Horizontal Well Technology Conference*, p. 8, Calgary, Alberta, Canada, 2002.

[15] A. F. Kuckes, R. T. Hay, J. McMahon, A. G. Nord, D. A. Schilling, and J. Morden, "New electromagnetic surveying/ranging method for drilling parallel horizontal twin wells," *SPE Drilling & Completion*, vol. 11, no. 2, pp. 85–90, 1996.

[16] R. M. Chen, Y. Chen, W. Luo, and B. G. Yin, "Application and development of MGT guiding technology in SAGD dual leve," *Xinjiang Oil and Gas*, vol. 7, no. 3, pp. 25–28, 2011.

[17] Q. Li, J. S. Li, C. M. Jiang, and H. W. Zhang, "SAGD horizontal well trajectory control technology in Fengcheng oilfield," *West-China Exploration Engineering*, vol. 27, no. 1, pp. 57-58, 2015.

[18] S. Chugh, R. Baker, A. Telesford, and E. Zhang, "Mainstream options for heavy oil:part I-cold production," *Journal of Canadian Petroleum Technology*, vol. 39, no. 4, p. 9, 2000.

[19] Z. Y. Wu, D. L. Gao, and B. B. Diao, "An investigation of electromagnetic anti-collision real-time measurement for drilling cluster wells," *Journal of Natural Gas Science and Engineering*, vol. 23, pp. 346–355, 2015.

[20] K. M. Churchill, C. Link, and C. C. Youmans, "A comparison of the finite-element method and analytical method for modeling unexploded ordnance using magnetometry," *IEEE Transactions on Geoscience and Remote Sensing*, vol. 50, no. 7, pp. 2720–2732, 2012.

[21] E. Thébault, C. C. Finlay, C. D. Beggan et al., "International geomagnetic reference field: the 12th generation," *Earth, Planets and Space*, vol. 67, no. 1, p. 79, 2015.

[22] A. Pignatelli, I. Nicolosi, R. Carluccio, M. Chiappini, and R. von Frese, "Graphical interactive generation of gravity and magnetic fields," *Computers & Geosciences*, vol. 37, no. 4, pp. 567–572, 2011.

[23] Z. Y. Guo, D. J. Liu, Q. Pan, Y. Y. Zhang, Y. Li, and Z. Wang, "Vertical magnetic field and its analytic signal applicability in oil field underground pipeline detection," *Journal of Geophysics and Engineering*, vol. 12, no. 3, pp. 340–350, 2015.

[24] Z. Y. Guo, D. J. Liu, Q. Pan, and Y. Y. Zhang, "Forward modeling of total magnetic anomaly over a pseudo-2D underground ferromagnetic pipeline," *Journal of Applied Geophysics*, vol. 113, pp. 14–30, 2015.

[25] Z. Y. Guo, D. J. Liu, Z. Chen, and H. Meng, "Modeling on ground magnetic anomaly detection of underground ferromagnetic metal pipeline," in *ICPTT 2012: Better Pipeline Infrastructure for a Better Life*, pp. 1011–1024, ASCE, 2012.

[26] D. J. Liu, Z. Y. Guo, H. Zhu, Q. Pan, and Q. H. Ai, "Voxel partitioning strategy of magnetic dipole reconstruction for underground ferrous pipeline magnetic anomaly," *Progress in Geophysics*, vol. 31, no. 6, pp. 2756–2761, 2016.

[27] S. H. Jiang, J. G. Hou, Y. M. He, and S. J. Wang, "Theoretical study and experimental verification of magnetic gradient tensor partial contraction using magnetic dipole," *Journal of Chinese Inertial Technology*, vol. 25, no. 4, pp. 473–477, 2017.

[28] A. J. Petruska and J. J. Abbott, "Optimal permanent-magnet geometries for dipole field approximation," *IEEE Transactions on Magnetics*, vol. 49, no. 2, pp. 811–819, 2013.

[29] S. D. Billings, C. Pasion, S. Walker, and L. Beran, "Magnetic models of unexploded ordnance," *IEEE Transactions on Geoscience and Remote Sensing*, vol. 44, no. 8, pp. 2115–2124, 2006.

[30] M. Marchetti, V. Sapia, and A. Settimi, "Magnetic anomalies of steel drums: a review of the literature and research results of the INGV," *Annals of Geophysics*, vol. 56, no. 1, article 0108, 2013.

[31] C. C. Finlay, S. Maus, C. D. Beggan et al., "International geomagnetic reference field: the eleventh generation," *Geophysical Journal International*, vol. 183, no. 3, pp. 1216–1230, 2010.